Core Temperature Estimation of Lithium-Ion Batteries Using Long Short-Term Memory (LSTM) Network and Kolmogorov-Arnold Network (KAN)

Dominic Karnehm[©], Graduate Student Member, IEEE, Akash Samanta[©], Graduate Student Member, IEEE, Christian Rosenmüller, Antje Neve, Member, IEEE, and Sheldon Williamson, Fellow, IEEE

Abstract—Health-conscious battery management systems (BMSs) that rely on surface temperature measurements are insufficient for managing automotive lithium-ion batteries (LIBs). Experimental studies have shown temperature differences of up to 10 °C between surface and core of cylindrical LIBs. BMSs that consider only surface temperature overlook critical thermal information. The missing monitoring can delay detecting thermal events within the cell, accelerating battery degradation and increasing the risk of thermal runaway. This article introduces two deep learning algorithms to address this: Kolmogorov-Arnold network (KAN) and interconnected long short-term memory (LSTM) network. Both approaches estimate the core temperature of LIBs without requiring surface temperature feedback to the neural network. Experimental validation revealed a core temperature mean absolute error (MAE) of 0.55 °C with a computational cost of 2.9-3.2 ms for KAN. The proposed interconnected LSTM reached a MAE of 0.80 °C. The performance of the two core temperature estimation techniques was further evaluated under dynamic loading profile using urban dynamometer driving schedule (UDDS) drive cycle. The KAN method achieved a MAE of 0.325 °C, demonstrating its adaptability to dynamic operating conditions. The two proposed methods, primarily KAN, are both adaptive and computationally efficient, making them suitable for integrating onboard BMS and cloud-enabled digital-twin-based BMS systems.

Index Terms—Battery management systems (BMSs), datadriven techniques, digital twining, electric vehicles (EVs), machine learning (ML), state estimation.

NOMENCLATURE

Battery current in A. Battery voltage in V. $T_{\rm amb}$ Ambient temperature in °C.

Received 4 January 2025; revised 6 March 2025; accepted 8 April 2025. Date of publication 10 April 2025; date of current version 24 July 2025. This work was supported in part by the Digitalization and Technology Research Center of the Bundeswehr (dtec.bw), in part by dtec.bw through European Union-NextGenerationEU, and in part by German Federal Ministry for Education and Research (BMBF) through the Project Open6GHub under Grant 16KISK003K. (Corresponding author: Dominic Karnehm.)

Dominic Karnehm and Antje Neve are with the Department of Electrical Engineering and Technical Informatics, University of the Bundeswehr Munich, 85577 Neubiberg, Germany (e-mail: dominic.karnehm@unibw.de;

Akash Samanta and Sheldon Williamson are with the Department of Electrical, Computer, and Software Engineering, Ontario Tech University, Oshawa, ON L1G 0C5, Canada.

Christian Rosenmüller is with the Institute for Sustainable Energy Systems (ISES), Munich University of Applied Sciences, 80335 Munich, Germany. Digital Object Identifier 10.1109/TTE.2025.3559633

 T_S Surface temperature of the battery in °C. $T_{\rm core}$ Core temperature of the battery in °C.

Time step n.

KAN activation function/function matrix.

Input vector.

Expected/predicted output vector. y/\hat{y}

ACRONYMS

ΑI Artificial intelligence. **BMS** Battery management system. EVs

Electric vehicles.

KAN Kolmogorov-Arnold network. **LSTM** Long short-term memory. MAE Mean absolute error. Coefficient of determination.

RMSE Root-mean-square error.

SOC State-of-charge. SOH State-of-health. SOT State-of-temperature.

I. Introduction

DOPTION of EVs hinges significantly on advancements A in battery life, safety, and effectiveness of TMS [1]. Effective thermal management ensures optimal battery performance across various climates, reduces degradation, and prevents overheating, which enhances both longevity and safety while maintaining higher resale values but also reduces overall ownership costs. Together, these factors contribute to making EVs more reliable, cost-efficient, and appealing, driving their broader acceptance and market expansion. Experimental studies and user experiences revealed that the performance, safety, and life of LIB are significantly affected by the operating temperature of LIB [2], [3]. Battery temperature outside of the safe operating region specified by the manufacturer results in accelerated battery degradation and often leads to safety issues such as thermal runaway or performance degradation [4], [5]. Such thermal issues become even more complicated in EVs battery packs typically consisting of several 100 and 1000 of individual cells closely packed, resulting in thermal imbalance exacerbated by inhomogeneous heating/cooling, particularly under fast charging/discharging

- D 0	36.11	35 117	T	D 6
Reference	Model	Model Input	Estimated Parameters	Performance
Lin et al. [7]	H_{∞} model	I, inlet coolant temperature	T_S, T_{core}	Worst case $\leq 3.1 ^{\circ}\text{C}$
Richardson et al. [8]	EKF-based estimator	I, V	Temperature distribution	$RMSE < 0.7 ^{\circ}C$
Chen et al. [9]	EKF-based estimator	I, V	T_S, T_{core}	$T_{core} \pm 1.5 ^{\circ}\mathrm{C}$
				$/T_S \pm [-0.5 ^{\circ}\text{C}; 1 ^{\circ}\text{C}]$
Schmidth et al. [10]	Impedance-based	EIS-Measurement, SOC	Bulk temperature	with SOC $\pm~0.17^{\circ}\mathrm{C}$
				without SOC $\pm~2.5^{\circ}\mathrm{C}$
Wang et al. [11]	LSTM with transfer learning	I, V, T_S, T_{amb}	T_{core}	$RMSE < 0.3302 ^{\circ}C$
				MAE $0.3302^{\circ}\mathrm{C}$
Zheng et al. [12]	LSTM	Impedance, I, V	volume-average temperature	RMSE $0.46^{\circ}\mathrm{C}$
Surya et al. [6]	2D grid LSTM	I,V,\dot{Q},T_S	T_{core}	$RMSE \le 0.81 ^{\circ}C$
Xu et al. [13]	Nonlinear Spatiotemporal Modeling	I, V	Temperature distribution	$RMSE \le 0.1439 ^{\circ}C$
Kleiner et al. [14]	ECM-NARX-network	SOC_{int} , I	T_{core}	$MSE < 0.5 ^{\circ}C$
Wei et al . [15]	LTNN-UKF	I, V	Temperature distribution	$RMSE \le 0.4266 ^{\circ}C$
				MAE $0.3180^{\circ}\mathrm{C}$
Zhang et al. [16]	LSTM	I, V, T_S	T_{core}	$RMSE \le 0.171 ^{\circ}C$
				$MAE \le 0.148 ^{\circ}C$
Zhang et al. [16]	GRU	I, V, T_S	T_{core}	$RMSE \le 0.131 ^{\circ}C$
				MAE 0.099 °C
Chin et al. [17]	Electro-Thermal State-Space model	I, T_{amb}	T_S, T_{core}	$T_S \text{ MSE} \leq 3 ^{\circ}\text{C}$

TABLE I
SUMMARY OF REFERENCES FOR TEMPERATURE ESTIMATION

and dynamic operations and conditions. Furthermore, a difference of up to 10 °C is noticed between surface and core temperature, especially in cylindrical LIB cells [6]. Therefore, closely monitoring the core temperature of individual cells is extremely important for effective TMS control, ensuring longer battery life and safer operation under dynamic operating conditions and fast charging of EVs batteries.

The representative studies on battery temperature estimations have been summarized in Table I. Zheng et al. [18] identified four key metrics for assessing the SOT of LIB: surface temperature, core temperature, bulk temperature, and temperature distribution. Traditionally, cell temperatures are monitored using sensors such as thermistors or thermocouples attached to the cell surface. However, in EVs, the battery pack consists of numerous cells, and equipping each cell with a temperature sensor significantly increases both cost and hardware complexity. Consequently, only a limited number of sensors are installed at key locations. For instance, the Chevy Volt employs 16 sensors for 288 cells, while the Ford C-Max Hybrid uses ten sensors for 76 cells [7]. This limited sensor deployment reduces full observability of individual cell temperatures. Moreover, even with surface temperature sensors, it is challenging to monitor the rapidly changing internal temperature of the cell due to the heat transfer delay from the core to the surface. As a result, temperature information obtained through direct sensor measurements often proves insufficient, leading to suboptimal thermal management in battery systems. Moreover, in cylindrical batteries, especially those under forced convection cooling or with larger diameters (e.g., 26 650 cells), the Biot number Bi is given by Bi = k/hL, where h is the heat transfer coefficient, L is the characteristic length, and k is the thermal conductivity [19], [20], can be greater than 0.1. This indicates significant thermal gradients within the battery. Consequently, the core temperature can be substantially higher than the surface temperature, with differences reaching up to 10 °C. Therefore, monitoring or accurately estimating the core temperature is critical for maintaining the thermal safety and performance of LIB.

Existing high-fidelity thermal models [20], [21] can predict the detailed temperature distribution throughout the cell. However, these models are not suitable for onboard applications due to their high computational intensity, especially for the entire battery pack consisting of 100-1000 of individual cells. Reduced order models [22], [23] are capable of estimating the bulk or average temperature and capturing the thermal dynamics of the cell. Even though these models are computationally efficient compared to detailed modeling, they often fail to capture the cell dynamics and are still not suitable for on-board application due to the commutative computational cost for the entire battery pack. Lumped thermal models [20], [24] are capable of estimating surface and core temperature simultaneously; however, such simplified models are not reliable in terms of accuracy and the capability of considering the cell dynamics. Moreover, in general, equivalent model-based estimation methods often fail to consider the dynamics of the operating conditions, such as variable load current, ambient temperature, and aging of the battery. These results in poor reliability over the entire cycle life of batteries, EVs despite high degree of accuracy during the laboratory conditions [25]. Numerical methods [8], [26], [27] such as finite element methods are also established to predict the battery temperature distribution even under dynamic operating conditions. Like distributed thermal models, numerical models are also computationally expensive, resulting in impractical for on-board BMS. Schmidt et al. [10], Srinivasan et al. [28], and Zheng et al. [12] used EIS-based internal temperature estimation of LIB. However, this is limited by the cost of the measurement system and integration of the EIS setup to the on-board BMS. Fusion of data-driven algorithms and lumped parameter thermal models [6], [9], [29] are also proposed for cell core temperature estimation, where the influence of heat generation rate and temperature entropy coefficient on the heat generation rate is considered to improve the estimation accuracy. However, these models still depend on the parameters of the lumped models, which change with battery aging and operating conditions.

The prediction of core temperature in LIB is inherently a time-series prediction problem due to the distributed parameter system with spatiotemporal variations [13]. In recent years, researchers have increasingly adopted AI and ML-based techniques to monitor and predict both short-term [30] and long-term [31] states of LIBs. For instance, Kleiner et al. [14] proposed a nonlinear autoregressive model with exogenous (NARX) inputs, Wei et al. [15] utilized a backpropagation neural network (BPNN), Wang et al. [11] employed a LSTM network, and Surya et al. [6] applied a 2-D grid LSTM for core temperature estimation. These studies primarily relied on battery current, voltage, SOC, and heat losses within each cell as inputs to their ML algorithms. RNNs are particularly adept at capturing long-term dependencies in time-series data by enabling information transfer across multiple time steps through recurrent connections within the network. However, training RNNs on extended sequences or large time-series datasets often encounters challenges such as vanishing or exploding gradients. To address these issues, Cho et al. [32] introduced the GRU. Recently, Yuan et al. [33] proposed a method combining a numerical model with an LSTM neural network for core temperature estimation. In this approach, the numerical model, utilizing EIS, provided volume-averaged temperature features for the LSTM network. While the method demonstrated an estimation MAE of less than 0.23 °C, it still faced the inherent challenges associated with numerical and EIS-based approaches, such as dependency on precise model parameters and operational constraints. Zhang et al. [16] performed a comparative analysis of RNN, LSTM, and GRU models, improving core temperature estimation performance through hyperparameter optimization using Bayesian optimization with a tree-structured Parzen Estimator, coupled with K-fold cross-validation. Despite these advancements, a common limitation of existing techniques is their dependence on measured surface temperature as feedback, necessitating a physical surface temperature sensor for each cell. Moreover, using heat generation as an input to ML models is impractical since obtaining accurate heat generation data is challenging in real-world applications. Heat generation cannot be directly measured, and estimations using equivalent thermal models become inaccurate over time due to battery aging and evolving model parameters influenced by varying operating conditions, including temperature fluctuations [17]. To address these research gaps, this article introduces a self-learnable KAN for predicting the internal and surface temperatures of LIBs, eliminating the need for a surface temperature sensor as feedback. The novel contributions of this work can be summarized in the following three aspects.

- First, the article introduced two LSTM and KAN for core and surface temperature estimation of LIB without needing any surface temperature measurement sensor feedback eliminating the need for a physical surface temperature sensor on each cell resulting in reduced cost and wire-harness of BMS.
- 2) The proposed core and surface temperature estimation techniques ensuring a high degree of prediction accuracy and reliability for a wide range of battery charging—discharging conditions and operating

- temperatures $(-20 \, ^{\circ}\text{C})$ to $40 \, ^{\circ}\text{C})$ even with dynamic drive cycle discharging conditions.
- 3) A comparative analysis between the proposed KAN and LSTM models to estimate core and surface temperature with state-of-the-art is also presented in this article to demonstrate the superiority and advantages of the proposed techniques for temperature monitoring and control by the on-board BMS.

The remainder of this article is organized as follows. Section II describes the methods employed, detailing the architectures of the proposed LSTM and KAN models. Section III outlines the experimental setup and data collection process used for model training and validation. Section IV presents the results and discusses the comparative analysis of the proposed techniques under various operating conditions. Finally, Section V concludes the article by summarizing the findings and providing insights for future research directions.

II. METHODS

As mentioned, multiple different temperature estimation methods have been proposed in the literature. This article introduced, for the first time, a KAN model for estimating the core and surface temperature of a LIB cell using the basic operating parameters of the battery: voltage, current, and ambient temperature. Also, an interconnected LSTM network architecture is proposed to estimate the core and surface temperature using the basic operating parameters. Sections II-A and II-B proposed the architecture of both introduced methods: the interconnected LSTM and the KAN architecture.

A. Interconnected LSTM

LSTM is a popular RNN, having a feedback connection within the model. The architecture makes LSTM well-suitable for processing time series data. Compared to other variations of RNN-based models like bidirectional LSTM (BiLSTM), conventional LSTM is less computationally intensive [34]. Moreover, as Lindemann et al. [35] demonstrated, LSTM networks are highly efficient in detecting anomalies and learning the temporal relationships within a time-dependent context. A single LSTM cell consists of an input gate i, forget gate f and the output gate o. The structure of a standard LSTM cell is illustrated in Fig. 1. The LSTM cell utilizes an input gate i, forget gate f, and the output gate o [36] to obtain the desired estimated parameters based on the input given to the model.

Previous studies have already presented estimation methods that use interconnected LSTM networks to estimate two parameters that are related to each other. The internal resistance of a battery cell is one of the most significant indicators of SOH. Van and Quang [37] of a previous study use this effect. Their work proposes a model architecture that estimates the SOH utilizing the input of temperature, current, and voltage. The interconnected network also employs the input of the first network and the output, the SOH. The authors conclude that estimating SOH as an input helps estimate internal resistances and their relationship is considered in the deep learning process of LSTM for improved precision.

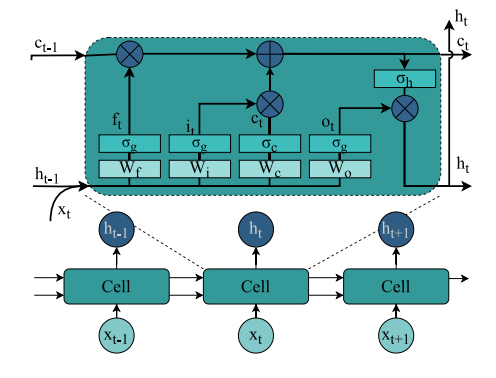


Fig. 1. LSTM Architecture and cell structure.

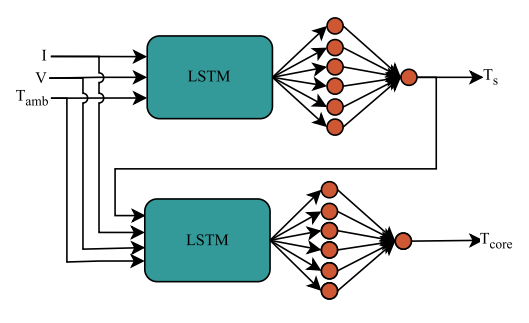


Fig. 2. Structure for estimating surface and core temperature using interconnected LSTM network.

In addition, Hu et al. [38] proposes a joined SOC and SOH estimation method using two interconnected LSTM networks. The positive results of the two studies indicate the potential of an interconnected LSTM for estimating interdependent states. This study introduces an interconnected LSTM designed to predict the surface temperature T_S and the core temperature T_{core} . The first network takes voltage V, current I, and ambient temperature $T_{\rm amb}$ as inputs, and its output is the surface temperature T_S . The second network uses the same inputs as the first and includes the surface temperature as an additional input parameter to estimate the core temperature $T_{\rm core}$. Fig. 2 illustrates the structure of the method. Each estimation model consists of an LSTM layer followed by a FNN with one hidden layer and a final output layer. Battery current I_t , voltage V_t , and ambient temperature $T_{amb,t}$ of i time steps are used as an input vector x of the LSTM network and as output vector y the estimated surface temperature T_{S,t_n} and core temperature T_{core,t_n} at time step t_n

$$x = \begin{bmatrix} I_{t_{n}}, I_{t_{n-1}}, \dots, I_{t_{n-i}}, \\ V_{t_{n}}, V_{t_{n-1}}, \dots, V_{t_{n-i}}, \\ T_{\text{amb},t_{n}}, T_{\text{amb},t_{n-1}}, \dots, T_{\text{amb},t_{n-i}} \end{bmatrix}$$
(1)
$$y = \begin{bmatrix} T_{S,t_{n}}, T_{\text{core},t_{n}} \end{bmatrix}.$$
(2)

B. Kolmogorov–Arnold Network

In MLP [39], during the learning process, the weights are optimized, and the activation function on each node is fixed. Unlike MLP, the KAN learns the activation function of each node [40] individually. The KAN does not have linear weights; it has univariable spliced functions. When a neuronal network learns a high-precision function, the model should learn to approximate the univariate functions and the compositional

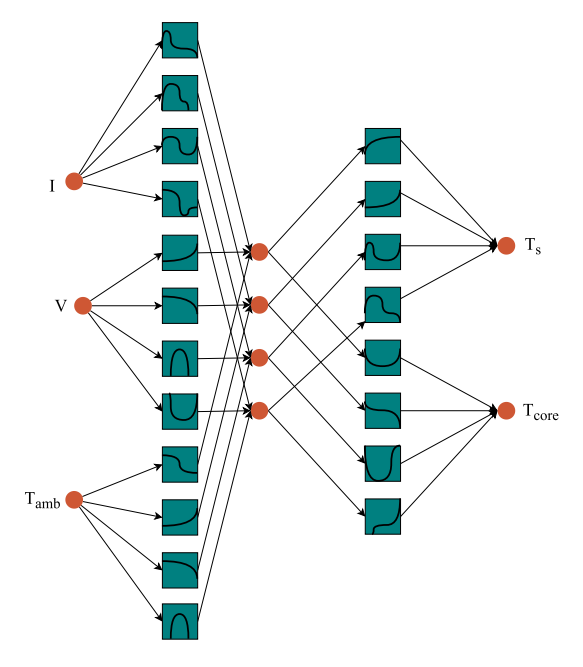


Fig. 3. Structure of a KAN

structure. The KAN, as proposed by Liu et al. [40], combines the splines and MLP to achieve a high degree of robustness, accuracy, and adaptability. Fig. 3 shows the structure of a KAN and the learnable activation functions as proposed in [40]. This article uses a similar architecture tailored to core and surface temperature estimation of LIB.

The KAN is inspired by the Kolmogorov-Arnold representation theorem [41]. The importance functions, and background calculus of the KAN architecture are discussed below

$$f(x) = f(x_1, \dots, x_n) = \sum_{q=1}^{2n+1} \Phi_q \left(\sum_{p=1}^n \phi_{q,p}(x_p) \right)$$
(3)

where $\phi_{q,p}: [0,1] \to \mathbb{R}$ and $\Phi_q: \mathbb{R} \to \mathbb{R}$. A single KAN activation value of the (l+1,j) neuron is the sum of all incoming postactivations, where l is the layer, j the neuron of the (l+1)th layer, and i the neuron of the lth layer [40]

$$x_{l+1,j} = \sum_{i=1}^{n_l} \phi_{l,j,i}(x_{l,i}), \quad j = 1, \dots, n_{l+1}.$$
 (4)

In matrix form, it can be defined as

$$\mathbf{x}_{l+1} = \underbrace{\begin{pmatrix} \phi_{l,1,1}(\cdot) & \cdots & \phi_{l,1,n_l}(\cdot) \\ \vdots & \ddots & \vdots \\ \phi_{l,n_{l+1},1}(\cdot) & \cdots & \phi_{l,n_{l+1},n_l}(\cdot) \end{pmatrix}}_{\Phi_t} \mathbf{x}_l$$
 (5)

where Φ_l is the function matrix of the lth KAN layer. A KAN network with L layers and a given input vector x is defined as

$$KAN(x) = (\Phi_{L-1} \circ \cdots \circ \Phi_1 \circ \Phi_0)x. \tag{6}$$

Previous studies [42], [43] have identified KAN as highly suitable for time-series data with a higher interdependency.

TABLE II
MOLICEL P42A INFORMATION

Property	Molicel P42A
Nominal Capacity	$4200\mathrm{mA}\mathrm{h}$
Continuous Discharge Rating (max)	$45\mathrm{A}$
Nominal Voltage	$3.6\mathrm{V}$
Maximum Voltage	$4.2\mathrm{V}$
Discharge cut-off Voltage	$2.5\mathrm{V}$
Discharge cut-off SOC	30%
Nominal discharge	$4\mathrm{A}$
Maximal discharge	$45\mathrm{A}$
Nominal charge	$2\mathrm{A}$
Maximal charge	$8.4\mathrm{A}$

These studies demonstrate the network's high interoperability and accuracy in predicting time-series data. Furthermore, compared to similar architectures used in estimation and prediction applications involving time-series data, such as MLP and LSTM, KAN achieves fewer parameters while maintaining higher or comparable accuracy. This work uses a tailored made KAN model to forecast the core and surface temperature of battery cells within one network. Battery current I_t , voltage V_t , and ambient temperature $T_{\text{amb},t}$ of three time steps t_n , t_{n-1} , and t_{n-2} are used as an input vector x of the network and as output vector y the estimated surface temperature T_{S,t_n} and core temperature T_{core,t_n} at time step t_n

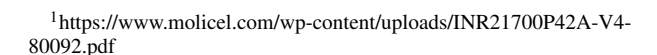
$$x = \begin{bmatrix} I_{t_{n}}, I_{t_{n-1}}, I_{t_{n-2}}, \\ V_{t_{n}}, V_{t_{n-1}}, V_{t_{n-2}}, \\ T_{\text{amb},t_{n}}, T_{\text{amb},t_{n-1}}, T_{\text{amb},t_{n-2}} \end{bmatrix}$$
(7)
$$y = \begin{bmatrix} T_{S,t_{n}}, T_{\text{core},t_{n}} \end{bmatrix}.$$
(8)

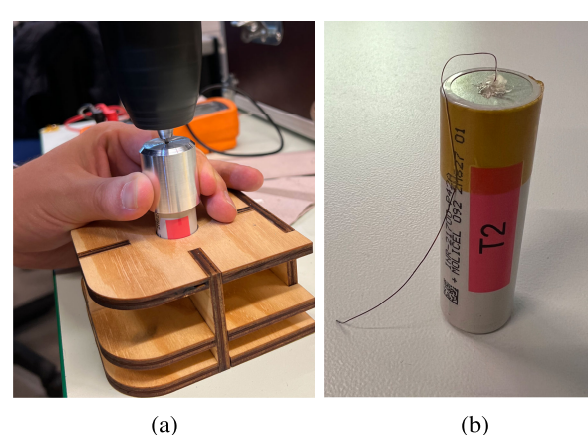
III. EXPERIMENTAL DATA AND MODEL TRAINING

A. Core Temperature Measurements

As shown in Fig. 4, the experimental setup collects the training, testing, and validation data for the proposed core and surface temperature estimation techniques. The battery testbench consists of an Ivium (Model: OctoStat5000) battery cycler, an Ivium (Model: OctoPDA-T) analog data collector for core and surface temperature measurement, a Binder environment control chamber (Model MKF 240), and an MCP (model: LBN-1990) digital power supply for providing power for core temperature measurement. A Microsoft Surface Pro 7 is used for the overall system control and centralized monitoring using the IviumSoft platform. A Molicel 4200 mAh 45 A INR-21700 cylindrical LIB is selected for this study. This battery was selected due to its fast response time, high maximum discharge, and current charge capability for fast discharge and charge cycling. The specification of the battery as provided in the manufacturer's data sheet is given in Table II.

At first, a physical temperature sensor (TE connectivity, GA10K3MCD1) is embedded at the core of each cell by drilling the cell vertically through the negative terminal of the cell. Before drilling, the cells were discharged to SOC 0% and cooled down at a temperature of 0 °C. The width of the drill is





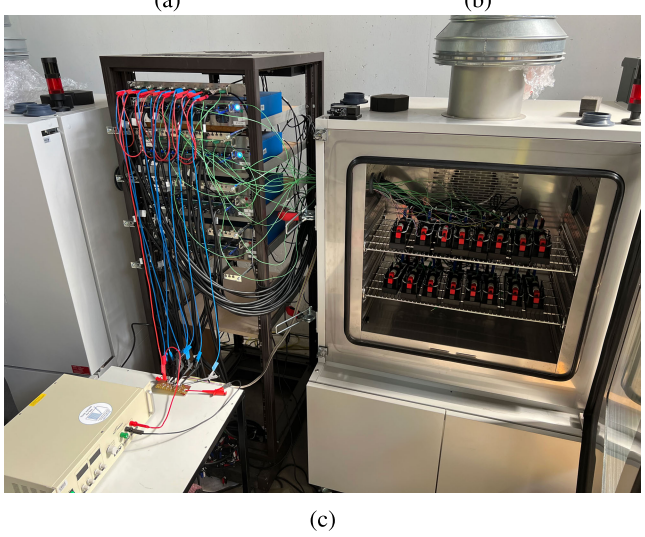


Fig. 4. Battery cell preparing. (a) Drilling of cooled down, discharged cell, (b) inserted core temperature sensor, and (c) battery cycling setup with cycler and climate chamber with seven prepared cells and nine validation cells.

0.55 mm, which is just sufficient for installing the temperature sensor as shown in Fig. 4(a). Then, the adhesive is provided carefully to seal the air gap and protect the battery's internal chemistry from degradation. Fig. 4(b) shows the prepared cell. The negative temperature coefficient (NTC) thermistors provide a measurement accuracy of $\pm 0.2~^{\circ}\text{C}$ at 20 $^{\circ}\text{C}$. A K-type thermocouple sensor is also installed on the surface of each cell for surface temperature measurement. The K-type sensor provide an accuracy of $\pm 2~^{\circ}\text{C}$ for temperatures between $-25~^{\circ}\text{C}$ and 40 $^{\circ}\text{C}$.

Then, a series of battery cycling is performed with four drilled cells and one validation cell in a wide range of ambient temperatures and C-rate as mentioned in the list below.

- 1) Ambient temperatures in performed order: 20 °C 10 °C, 0 °C, -10 °C, -20 °C, 30 °C, 40 °C.
- 2) 3× Each: CC-CV (0.3 C/0.3 C); CC-CV (0.5 C/0.5 C); CC-CV (0.8 C/0.8 C); CC-CV (1 C/1 C).

After a change in the outside temperature, a break of at least 3 h was taken to ensure that the cell rested under the changed temperature. The measured core and surface temperature at 20 °C, including cell voltage and current over 12 charging and discharging cycles, is shown in Fig. 5. Similarly, all the experiments are conducted per the schedule mentioned above to generate a large data set. The collected data are used

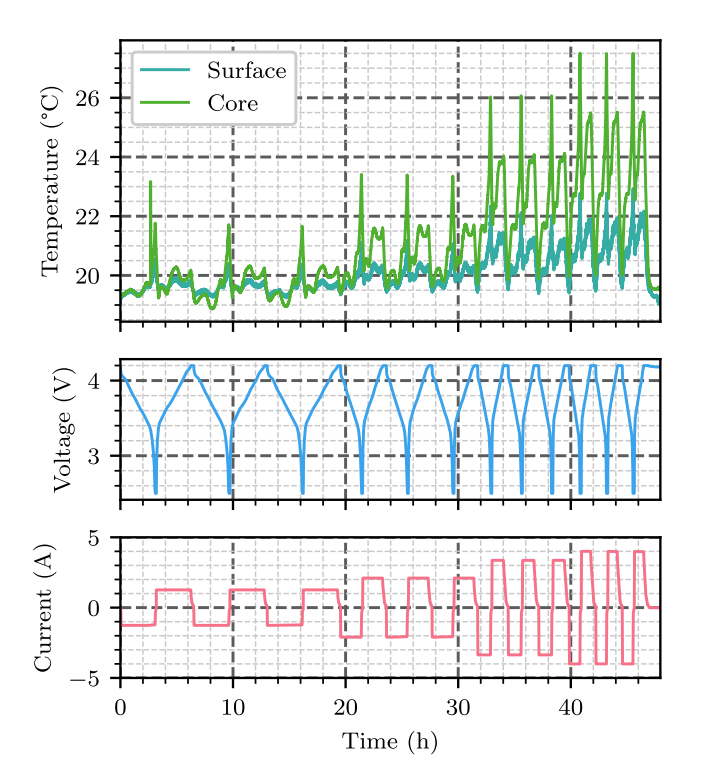


Fig. 5. Measurement data 20 °C ambient temperature.

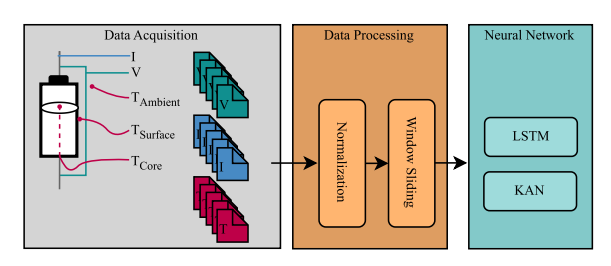


Fig. 6. Schematic layout of data and information flow followed in this study.

for both the LSTM and KAN network development, training, testing, and validation. The measured core and surface temperature data are then used as baseline and reference data to assess the prediction models' accuracy and generalization under varied ambient temperatures and C-rate. The measured temperature data are also used to compare the LSTM and KAN to demonstrate the proposed method's superiority and practicality.

B. Model Implementation and Validation

The flow of data acquisition, processing, and the neuronal network is illustrated in Fig. 6.

1) Data Processing: The test setup and the software used during data acquisition ensured no missing data points. In addition, the measurement software has already corrected for outliers in the data. Data processing consists of min-max normalization of the features. Furthermore, to preprocess the data for training and validation. To ensure that data are not considered by the model during training and validation, it is randomly divided into training and validation data-based ambient temperature and cell. At each ambient temperature, one out of four cells is randomly chosen as test cell and three

TABLE III
ARCHITECTURE OF MODELS

Layer	LSTM	KAN
1	LSTM(input=3, hidden size = 25, layers = 1)	KAN(9)
2	Dense(32)	KAN(32)
3	Dense(1)	KAN(16)
4	LSTM(input=4, hidden size = 50, layers = 1)	KAN(2)
5	Dense(32)	
6	Dense(1)	

cells for training. Data have been sliced into time windows of 5 s measurement, corresponding to 50 data points.

2) Model Implementation: Python 3.10 has been used as a programming language, PyTorch 2.3.1, and the KAN implementation of pykan 0.0.5 to implement the models. A grid search was carried out to determine the hyperparameters of the two network architectures. To determine the LSTM hyperparameters, an exploration via grid search was performed across different hidden layers (ranging from 1 to 3) and hidden sizes (25, 50, and 75) for each of the LSTM estimation networks. The evaluated hyperparameters of the KAN are the layer size of the two hidden layers of the network. The exploration includes the combinations 8/4, 16/8, 32/16, and 64/32 for the two layers. Table III presents the structures of the two selected hyperparameter configurations.

IV. RESULTS AND DISCUSSION

The performance and the superiority of the proposed KAN-based core and surface temperature estimation technique for LIB are demonstrated in this article through a detailed comparative analysis with the proposed LSTM model. Hyperparameter optimization was followed by training and validating each model. Two different datasets were utilized for independent training and evaluation. First, the above-mentioned dataset was measured during the core temperature experiments, as described in Section III-A, and is named the CC-CV dataset. Samata and Williamson [44] proposed a dataset containing measurements of CC-CV cycles up to 4 C at ambient temperatures -20 °C-40 °C, and urban dynamometer driving schedule (UDDS) and highway fuel economy driving schedule (HWFET) drive cycle at 25 °C 30 °C, and 40 °C ambient temperature employing Samsung INR21700-40T cylindrical cells, following named as drive cycle dataset. For training the measurements of CC-CV cycles, HWFET and UDDS are employed. The dataset contains data with a measurement frequency of 1 Hz. The model is evaluated once with the UDDS driving cycle at 25 °C and once more with HWFET 30 °C. In this case, the corresponding driving cycle is excluded from the respective training. Performance assessment was done with a new data set entirely unknown to both models. Three commonly referred metrics are chosen to quantitatively characterize the performance of the model, including RMSE, MAE, and coefficient of determination (R^2) , which can be described as follows:

$$RMSE = \sqrt{\sum_{i=1}^{n} \frac{\left(\hat{y}_i - y_i\right)^2}{n}}$$
 (9)

TABLE IV ${\rm MAE,~RMSE,~and~} R^2 {\rm ~Core~and~Surface~Temperature~Per~Model} \\ {\rm ~of~Drilled~Cells~in~^{\circ}C}$

	KAN	LSTM
MAE		
Core	0.579	0.613
Surface	0.353	0.370
RMSE		
Core	0.814	0.875
Surface	0.519	0.520
R^2		
Core	0.99808	0.99779
Surface	0.99911	0.99910

TABLE V $\label{eq:mae} \text{MAE Surface and Core Temperature Per Model in } ^{\circ}\text{C}$

	Surface		Core	
Ambient Temperature	KAN	LSTM	KAN	LSTM
40	0.230	0.293	0.464	0.768
30	0.363	0.473	1.403	1.143
20	0.325	0.264	0.207	0.419
10	0.403	0.413	0.714	0.639
0	0.267	0.306	0.532	0.528
-10	0.375	0.362	0.285	0.355
-20	0.422	0.432	0.493	0.571

$$MAE = \frac{1}{n} \sum_{i=1}^{n} |\hat{y}_i - y_i|$$
 (10)

$$R^{2} = \frac{\sum_{i=1}^{n} (y_{i} - \bar{y})^{2}}{\sum_{i=1}^{n} (y_{i} - \hat{y}_{i})^{2}} \quad \bar{y} = \frac{1}{n} \sum_{i=1}^{n} y_{i}$$
 (11)

where *n* is the sample size, y_i is the actual value, and $\hat{y_i}$ is the predicted value.

A. CC-CV Dataset

Table IV shows the model validation performance for both surface and core temperature estimation. The quantitative performance metrics of the model at the full range of ambient temperatures are performed for both LSTM and KAN-based surface and core temperature estimation algorithms. The KAN model is considered the model with the best performance for all analyzed metrics. From Table IV, it can be noticed that the average RMSE and MAE of core temperature measurement using KAN are less than 0.75 °C and 0.47 °C, respectively. Similarly, the average RMSE and MAE of surface temperature measurement using KAN is less than 0.47 °C and 0.30 °C, respectively.

The validation and robustness of the KAN and LSTM are also performed at a wide range of ambient temperatures, as shown in Table V. It can be noticed that the changes in MAE vary for KAN in the range of 0.230 °C at 40 °C to 0.422 °C at -20 °C for surface temperature estimation. Similarly, in KAN core temperature estimation, the MAE varies in the range of 0.207 °C at 20 °C and 1.40 °C at 30 °C. LSTM produced the slightest error of 0.355 °C at -10 °C for core temperature estimation, whereas for surface temperature, LSTM produced the least MAE of 0.293 °C at 40 °C.

The estimated surface and core temperatures are shown in Figs. 7 and 8, respectively, at 10 °C ambient temperature. As illustrated in Fig. 7 for the surface and Fig. 8 for the core,

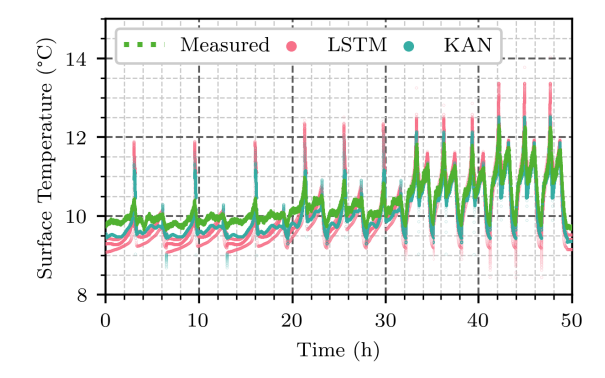


Fig. 7. Measured surface temperature (green) compared with KAN (cyan) and LSTM (pink) estimation models at 10 °C ambient temperature.

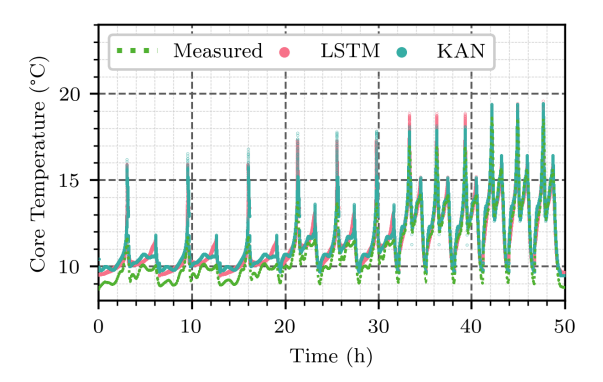


Fig. 8. Measured core temperature (green) compared with KAN (cyan) and LSTM (pink) estimation models at 10 $^{\circ}\text{C}$ ambient temperature.

the estimated temperatures closely match the measured values. A summary of MAE, RMSE, and R^2 of both core and surface temperature estimation using KAN and LSTM is shown in Table IV.

The estimated surface temperature based on the same input battery parameters, voltage, current, and ambient temperature is shown throughout the validation cell in Fig. 9. The validation cell has not been drilled and does not include a core temperature sensor. This enables the validation of model accuracy for a standard battery cell. The figure illustrates that higher maximum errors can be observed at lower ambient temperatures. A decrease in accuracy during aging cannot be observed. Furthermore, a significant relation between MAE and aging and temperature cannot be observed. As the zoomin illustrates, the KAN model shows higher accuracies than the LSTM model. The illustrated error shows significantly higher estimations than the measured values through short periods. The performance of the KAN and LSTM model within the validation cell is shown in Table VI. A reduction in accuracy compared to the drilled cells, shown in Table IV, can be seen. This apparent difference in accuracy between cells with and without an inserted temperature sensor can be explained by the physical effect on the cell caused by the insertion of the sensor.

Fig. 10 shows the measured capacity of the battery cells during the test period. The respective ambient temperatures are also shown. During the experiment, a capacity drop across all battery cells is seen. However, the validation cell shows

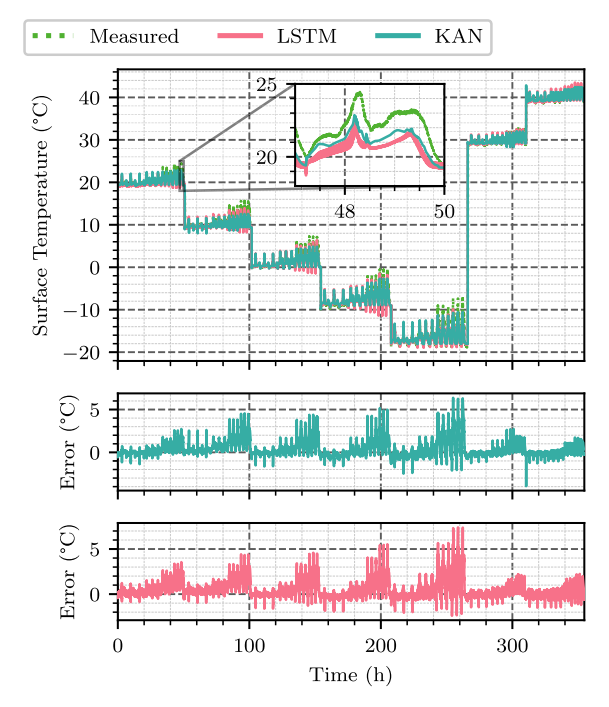


Fig. 9. Validation of surface temperature estimation method using validation cell over the wide range of ambient temperatures.

TABLE VI MAE, RMSE, and \mathbb{R}^2 Surface Temperature Per Model of Validation Cell in °C

	KAN	LSTM
MAE	0.550	0.800
RMSE	0.851	1.128
R^2	0.99793	0.99635

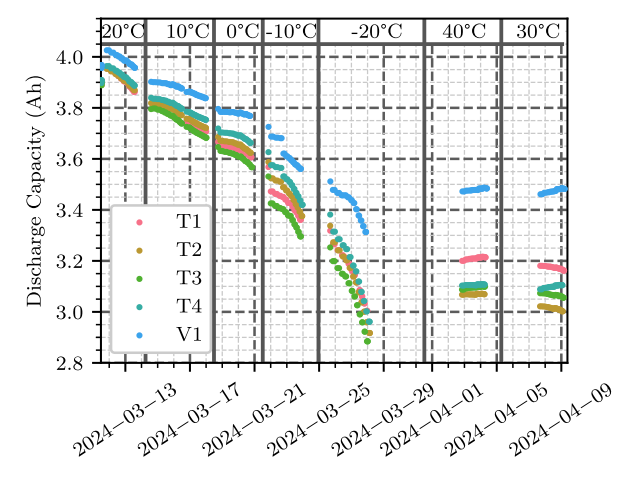


Fig. 10. Change of discharge capacity during performed experiments; Comparison between not prepared validation cell V1 and drilled test cells T1-T4.

a significantly lower capacity loss than cells with the core temperature sensor inserted.

B. Drive Cycle Dataset

Table VII shows the accuracy of the KAN and LSTM models trained with the dataset proposed in [44]. Due to the low standard deviation in core and surface temperature, the R^2 value is not considered reliable, given the inherent

TABLE VII

MAE AND RMSE CORE AND SURFACE TEMPERATURE PER MODEL AT UDDS DATASET AT VARIATIONS OF TRAINING IN °C

	UDDS 25 °C		UDDS 25 ° C (Unknown UDDS profile)		<i>HWFET</i> 30 °C	
	KAN	LSTM	KAN	LSTM	KAN	LSTM
MAE						
Core	0.610	0.901	0.598	0.887	0.936	0.727
Surface	0.411	1.206	0.481	1.030	0.775	0.725
RMSE						
Core	0.735	1.354	0.787	1.433	1.507	1.150
Surface	0.520	1.459	0.677	1.636	1.305	1.007

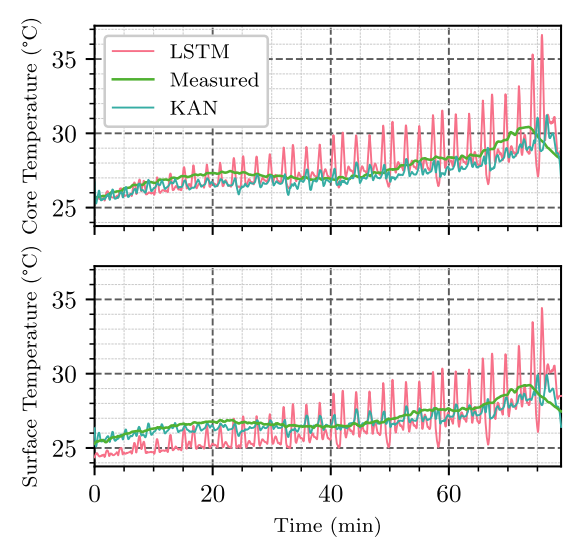


Fig. 11. Measured core and surface temperature (green) compared with KAN (cyan) and LSTM (pink) estimation models at UDDS 25 °C.

weaknesses associated with limited-variance data. The table gives MAE and RMSE of core and surface temperature estimation of three different training and validation settings as follows.

- 1) UDDS 25 °C: Training: CC-CV cycles, UDDS (30 °C, 40 °C), HWFET (25 °C, 30 °C, 40 °C); Validation: UDDS 25 °C.
- UDDS 25 °C (Unknown UDDS profile): Training: CC-CV cycles, HWFET (25 °C, 30 °C, 40 °C); Validation: UDDS 25 °C.
- 3) *HWFET* 30 °C: Training: CC-CV cycles, UDDS (25 °C, 30 °C, 40 °C), HWFET (25 °C, 40 °C); Validation: HWFET 30 °C.

For the UDDS driving cycle, KAN shows a better result than LSTM for all key performance indicators considered. With an RMSE of 0.677 °C for the surface temperature, there is only a slightly worse result of 0.157 °C RMSE between the results where the driving cycle is already known to the model, as it is included in the training data at other temperatures and the results where the driving cycle is still completely unknown. At HWFET, the LSTM model indicates that 1.150 °C and 1.007 °C RMSE have better core and surface temperature estimation performance, respectively.

Fig. 11 illustrates measured (green) and estimated KAN in cyan and LSTM in pink, core and surface temperature UDDS drive cycle at 25 °C, where training data include UDDS drive cycle at 30 °C and 40 °C. The figure shows a surface and

TABLE VIII

COMPUTATIONAL COST COMPARISON OF MODELS AND DIFFERENT HARDWARE SETUPS IN ms

CPU-Setup	LSTM	KAN
Intel Xeon Gold 6338 2G	0.55 ± 0.10	2.92 ± 0.45
Intel Core i9-10885H	0.58 ± 0.04	3.28 ± 0.34

core temperature increase of 4.0 °C and 4.9 °C. The proposed KAN model reproduces the battery behaviors and dynamics more accurately than the interconnected LSTM. Both models modulate the increasing temperatures. However, LSTM shows a significantly higher fluctuation in temperatures, which does not correctly reflect the dynamics of the battery. The KAN also shows higher dynamics compared to the measured temperature, although these are lower than in the LSTM.

C. Computational Cost

As can be seen from Table VIII, the computational cost at 20 °C, LSTM performs better than KAN with the CPU-setup with a computational cost in the range of 0.55–0.58 ms for LSTM whereas 2.92 to 3.28 ms for KAN. However, it is noticed that the computational cost can be reduced with improved CPU setup. Furthermore, the KAN implementation is still in a relatively early stage of development. Due to further development and the associated optimization of the implementation, performance gains can be expected over the coming months and years.

While KAN offers potentially greater predictive power and flexibility, especially in handling complex nonlinear relationships, these advantages come at the cost of increased computational complexity and time compared to the proposed LSTM model. The validation using the unprocessed validation cell influences the battery behavior. Future studies will enhance this by refining the insertion procedure. However, the results indicated that it is possible to minimize this influence as early as the modeling stage.

V. CONCLUSION AND OUTLOOK

This article introduces two neural network architectures to estimate the surface and core temperature of LIB employing voltage, current, and ambient temperature as model inputs. The proposed interconnected LSTM architecture can estimate the interdependent parameters, surface and core temperature, in time-series data. Learnable activation functions in neural networks offer a promising alternative to the traditional multilayer perceptron. The proposed KAN architecture utilizes this innovative approach to estimate core and surface temperatures for battery state estimation. First, core temperature measurements with Molicel P42A were performed to evaluate the proposed models. Furthermore, the dataset Zhang et al. [16] was used to evaluate the accuracy at dynamic conditions.

Some major findings include the following.

- 1) Battery cell preparation influences capacity reduction significantly.
- With computational cost of 0.55/0.58 ms, the LSTM model outperforms KAN (2.92/3.28 ms) by more than five times.

- 3) At CC-CV dataset, an MAE of 0.353 °C and 0.579 °C is noticed for surface and core temperature estimation with the KAN model, respectively.
- 4) At UDDS, drive cycle conditions KAN reaches an MAE of up to 0.411 °C and 0.610 °C of surface and core temperature, respectively. Interconnected LSTM outperforms KAN at HWFET drive cycle.

The results demonstrate the potential of both methods, especially the KAN model. For use in real-time applications, the lower computing time of LSTM can be an advantage over the lower accuracy, as seen in the most validation results. Thereby, LSTM HWFET drive cycle results indicate further investigations for real world settings. The estimation frequency required in combination with the number of cells to be monitored must be considered. The simultaneous estimation of core and surface temperature demonstrates its potential when compared to the methods listed in Table III. Previous methods leak in the possibility to estimate core and surface temperature at once. The suggested approach notably decreases the quantity of sensors needed for practical use. The surface temperature is not a parameter in estimating the core temperature. To evaluate the influence of aging in accuracy, future experiments should be carried out at the constant temperature. To improve the model, a hybrid model of physical thermal model and ML model has to be implemented based on the insight gained from this work. The models must be adapted to estimate the temperatures for large-scale battery pack applications implemented in on-board and cloud-based BMS.

REFERENCES

- [1] C. Bibin, M. Vijayaram, V. Suriya, R. Sai Ganesh, and S. Soundarraj, "A review on thermal issues in li-ion battery and recent advancements in battery thermal management system," *Mater. Today, Proc.*, vol. 33, pp. 116–128, Jan. 2020.
- [2] F. Leng, C. M. Tan, and M. Pecht, "Effect of temperature on the aging rate of Li ion battery operating above room temperature," *Sci. Rep.*, vol. 5, no. 1, p. 12967, Aug. 2015.
- [3] C. Chetri, A. Samanta, and S. Williamson, "Critical understanding of temperature gradient during fast charging of lithium-ion batteries at low temperatures," in *Proc. 49th Annu. Conf. IEEE Ind. Electron. Soc.*, Oct. 2023, pp. 1–6.
- [4] J. S. Edge et al., "Lithium ion battery degradation: What you need to know," Phys. Chem. Chem. Phys., vol. 23, no. 14, pp. 8200–8221, 2021.
- [5] X. Feng, M. Ouyang, X. Liu, L. Lu, Y. Xia, and X. He, "Thermal runaway mechanism of lithium ion battery for electric vehicles: A review," *Energy Storage Mater.*, vol. 10, pp. 246–267, Jan. 2018.
- [6] S. Surya, A. Samanta, V. Marcis, and S. Williamson, "Hybrid electrical circuit model and deep learning-based core temperature estimation of lithium-ion battery cell," *IEEE Trans. Transport. Electrific.*, vol. 8, no. 3, pp. 3816–3824, Sep. 2022.
- [7] X. Lin, H. E. Perez, J. B. Siegel, and A. G. Stefanopoulou, "Robust estimation of battery system temperature distribution under sparse sensing and uncertainty," *IEEE Trans. Control Syst. Technol.*, vol. 28, no. 3, pp. 753–765, May 2020.
- [8] R. R. Richardson, S. Zhao, and D. A. Howey, "On-board monitoring of 2-D spatially-resolved temperatures in cylindrical lithium-ion batteries: Part II. State estimation via impedance-based temperature sensing," *J. Power Sources*, vol. 327, pp. 726–735, Sep. 2016.
- [9] L. Chen et al., "Core temperature estimation based on electro-thermal model of lithium-ion batteries," *Int. J. Energy Res.*, vol. 44, no. 7, pp. 5320–5333, Jun. 2020.
- [10] J. P. Schmidt, S. Arnold, A. Loges, D. Werner, T. Wetzel, and E. Ivers-Tiffée, "Measurement of the internal cell temperature via impedance: Evaluation and application of a new method," *J. Power Sources*, vol. 243, pp. 110–117, Dec. 2013.

- [11] N. Wang et al., "Core temperature estimation method for lithium-ion battery based on long short-term memory model with transfer learning," *IEEE J. Emerg. Sel. Topics Power Electron.*, vol. 11, no. 1, pp. 201–213, Feb. 2023.
- [12] Y. Zheng et al., "Real-time sensorless temperature estimation of lithiumion batteries based on online operando impedance acquisition," *IEEE Trans. Power Electron.*, vol. 39, no. 10, pp. 13853–13868, Oct. 2024.
- [13] K.-K. Xu, H.-X. Li, and H.-D. Yang, "Local-properties-embedding-based nonlinear spatiotemporal modeling for lithium-ion battery thermal process," *IEEE Trans. Ind. Electron.*, vol. 65, no. 12, pp. 9767–9776, Dec. 2018.
- [14] J. Kleiner, M. Stuckenberger, L. Komsiyska, and C. Endisch, "Real-time core temperature prediction of prismatic automotive lithium-ion battery cells based on artificial neural networks," *J. Energy Storage*, vol. 39, Jul. 2021, Art. no. 102588.
- [15] Z. Wei et al., "Machine learning-based hybrid thermal modeling and diagnostic for lithium-ion battery enabled by embedded sensing," *Appl. Thermal Eng.*, vol. 216, Nov. 2022, Art. no. 119059.
- [16] X. Zhang, H. Xiang, X. Xiong, Y. Wang, and Z. Chen, "Benchmarking core temperature forecasting for lithium-ion battery using typical recurrent neural networks," *Appl. Thermal Eng.*, vol. 248, Jul. 2024, Art. no. 123257.
- [17] C. S. Chin, Z. Gao, and C. Z. Zhang, "Comprehensive electro-thermal model of 26650 lithium battery for discharge cycle under parametric and temperature variations," *J. Energy Storage*, vol. 28, Apr. 2020, Art. no. 101222.
- [18] Y. Zheng, Y. Che, X. Hu, X. Sui, D.-I. Stroe, and R. Teodorescu, "Thermal state monitoring of lithium-ion batteries: Progress, challenges, and opportunities," *Prog. Energy Combustion Sci.*, vol. 100, Jan. 2024, Art. no. 101120.
- [19] S. Al Hallaj, H. Maleki, J. S. Hong, and J. R. Selman, "Thermal modeling and design considerations of lithium-ion batteries," *J. Power Sources*, vol. 83, nos. 1–2, pp. 1–8, Oct. 1999.
- [20] C. Forgez, D. V. Do, G. Friedrich, M. Morcrette, and C. Delacourt, "Thermal modeling of a cylindrical LiFePO₄/graphite lithium-ion battery," *J. Power Sources*, vol. 195, no. 9, pp. 2961–2968, May 2010.
- [21] B. Fan, B. Zhang, Y. Shi, and Y. Chang, "A high-fidelity lithium-ion battery emulator for electric vehicle application," *Sci. Rep.*, vol. 14, no. 1, p. 19742, Aug. 2024.
- [22] R. Mahamud and C. Park, "Reciprocating air flow for li-ion battery thermal management to improve temperature uniformity," *J. Power Sources*, vol. 196, no. 13, pp. 5685–5696, Jul. 2011.
- [23] P. T. Coman, E. C. Darcy, B. Strangways, and R. E. White, "A reduced-order lumped model for li-ion battery packs during operation," *J. Electrochemical Soc.*, vol. 168, no. 10, Oct. 2021, Art. no. 100525.
- [24] C. Park and A. K. Jaura, "Dynamic thermal model of li-ion battery for predictive behavior in hybrid and fuel cell vehicles," SAE Tech. Paper 2003–01–2286, 2003.
- [25] L. Xiang, C. W. Lee, O. Zikanov, and C.-C. Hsu, "Efficient reduced order model for heat transfer in a battery pack of an electric vehicle," *Appl. Thermal Eng.*, vol. 201, Jan. 2022, Art. no. 117641.
- [26] G. Guo, B. Long, B. Cheng, S. Zhou, P. Xu, and B. Cao, "Three-dimensional thermal finite element modeling of lithium-ion battery in thermal abuse application," *J. Power Sources*, vol. 195, no. 8, pp. 2393–2398, Apr. 2010.
- [27] S. Du et al., "Study on the thermal behaviors of power lithium iron phosphate (LFP) aluminum-laminated battery with different tab configurations," *Int. J. Thermal Sci.*, vol. 89, pp. 327–336, Mar. 2015.
- [28] R. Srinivasan, B. G. Carkhuff, M. H. Butler, and A. C. Baisden, "Instantaneous measurement of the internal temperature in lithium-ion rechargeable cells," *Electrochimica Acta*, vol. 56, no. 17, pp. 6198–6204, Jul. 2011.
- [29] D. Li and L. Yang, "Identification of spatial temperature gradient in large format lithium battery using a multilayer thermal model," *Int. J. Energy Res.*, vol. 44, no. 1, pp. 282–297, Jan. 2020.
- [30] J. Tian, C. Chen, W. Shen, F. Sun, and R. Xiong, "Deep learning framework for lithium-ion battery state of charge estimation: Recent advances and future perspectives," *Energy Storage Mater.*, vol. 61, Aug. 2023, Art. no. 102883.
- [31] K. Li, Y. Wang, and Z. Chen, "A comparative study of battery state-of-health estimation based on empirical mode decomposition and neural network," J. Energy Storage, vol. 54, Oct. 2022, Art. no. 105333.
- [32] K. Cho et al., "Learning phrase representations using RNN encoder– decoder for statistical machine translation," 2014, arXiv:1406.1078.

- [33] A. Yuan, T. Cai, H. Luo, Z. Song, and B. Wei, "Core temperature estimation of lithium-ion battery based on numerical model fusion deep learning," *J. Energy Storage*, vol. 102, Nov. 2024, Art. no. 114148.
- [34] S. Siami-Namini, N. Tavakoli, and A. S. Namin, "The performance of LSTM and BiLSTM in forecasting time series," in *Proc. IEEE Int. Conf. Big Data*, Dec. 2019, pp. 3285–3292.
- [35] B. Lindemann, B. Maschler, N. Sahlab, and M. Weyrich, "A survey on anomaly detection for technical systems using LSTM networks," *Comput. Ind.*, vol. 131, Oct. 2021, Art. no. 103498.
- [36] S. Hochreiter and J. Schmidhuber, "Long short-term memory," Neural Comput., vol. 9, no. 8, pp. 1735–1780, 1997.
- [37] C. Nguyen Van and D. T. Quang, "Estimation of SoH and internal resistances of lithium ion battery based on LSTM network," *Int. J. Electrochemical Sci.*, vol. 18, no. 6, Jun. 2023, Art. no. 100166.
- [38] P. Hu, W. F. Tang, C. H. Li, S.-L. Mak, C. Y. Li, and C. C. Lee, "Joint state of charge (SOC) and state of health (SOH) estimation for lithiumion batteries packs of electric vehicles based on NSSR-LSTM neural network," *Energies*, vol. 16, no. 14, p. 5313, Jul. 2023.
- [39] S. Haykin, Neural Networks: A Comprehensive Foundation. Hoboken, NJ, USA: Prentice-Hall PTR, 1998.
- [40] Z. Liu et al., "KAN: Kolmogorov-arnold networks," 2024, arXiv:2404.19756.
- [41] A. N. Kolmogorov, "On the representation of continuous functions of many variables by superposition of continuous functions of one variable and addition," in *Proc. Doklady Akademii Nauk*, 1957, vol. 114, no. 5, pp. 953–956.
- [42] M. Liu, S. Bian, B. Zhou, and P. Lukowicz, "IKAN: Global incremental learning with KAN for human activity recognition across heterogeneous datasets," 2024, arXiv:2406.01646.
- [43] C. J. Vaca-Rubio, L. Blanco, R. Pereira, and M. Caus, "Kolmogorovarnold networks (KANs) for time series analysis," 2024, arXiv:2405.08790.
- [44] A. Samanta and S. Williamson, "Cloud-integrated adaptive deep learning framework for real-time battery core temperature estimation and enhanced thermal safety," Tech. Rep., 2025.



Dominic Karnehm (Graduate Student Member, IEEE) received the B.Sc. degree in information system and management and the M.Sc. degree in computer science from Munich University of Applied Sciences, Munich, Germany, in 2019 and 2021, respectively. He is a Ph.D. Candidate with the professorship for Internet of Things, University of the Bundeswehr Munich, Munich.

His research interests include cloud computing and IoT in the field of electric vehicles, digital twinning of battery management systems, and applications of

machine learning in the field of batteries.



Akash Samanta (Graduate Student Member, IEEE) received the B.Tech. degree (Hons.) in electrical engineering from West Bengal University of Technology, Kolkata, India, in 2012, and the M.Tech. (Hons.) and M.B.A. degrees in electrical engineering and energy management from the University of Calcutta, Kolkata, in 2018 and 2014, respectively. He is currently pursuing the Ph.D. degree with the Department of Electrical, Computer, and Software Engineering, Ontario Tech University, Oshawa, ON, Canada.

From 2014 to 2018, he was a Project Officer and Solar Energy Master Trainer with the Department of Energy Management, Indian Institute of Social Welfare and Business Management, Kolkata. His research interests include digital twinning of battery management systems, automotive energy storage, power electronics converters, and the application of machine learning and artificial intelligence.



Christian Rosenmüller received the B.Eng. degree in electrical engineering–electrical and information technology from Munich University of Applied Sciences (MUAS), Munich, Germany, in 2019, and the M.Sc. degree in electrical engineering from MUAS, in 2021.

In 2021, he embarked on his doctoral studies as a Research Assistant, funded as part of a public research program, Institute for Sustainable Energy Systems (ISES) in the research area of the Electrical Energy Storage Research Group, Munich. His focus

is on the online impedance measurement and impedance-based diagnostics.



Antje Neve (Member, IEEE) received the Diploma degree from the University of Applied Sciences, Dresden, Germany, in 2004, the M.Sc. degree in computer science from the Technical University of Munich, Munich, Germany, in 2005, and the Ph.D. degree from the Technical University of Munich, in 2009, in cooperation with BMW Research and Development, focusing on developing object detection algorithms for driver assistant systems.

She then continued her career as a Satellite Software Engineer with Airbus Defence and Space,

Stevenage, UK, working on Galileo Satellites and then returned to BMW as a Project Manager and Software Architect for the instrument cluster and driver camera. Passionate about teaching and guiding young people, she has held the professorship for Internet of Things with the University of the Bundeswehr Munich, Munich, since 2020, teaching computer and data science, robotics and sensors, and Internet of Things. Her research interests include applied data processing, cloud computing, didactics of computer science and anything that makes the world a better place in combining bringing out the best in people and using technology.



Sheldon Williamson (Fellow, IEEE) received the B.E. degree (Hons.) in electrical engineering from the University of Mumbai, Mumbai, India, in 1999, and the M.S. and Ph.D. degrees (Hons.) in electrical engineering from Illinois Institute of Technology, Chicago, IL, USA, in 2002 and 2006, respectively.

He is currently a Professor with the Department of Electrical, Computer, and Software Engineering and the Director of Smart Transportation Electrification and Energy Research (STEER) Group, Faculty of Engineering and Applied Sciences, Ontario Tech

University, Oshawa, ON, Canada. He holds the prestigious NSERC Canada Research Chair position in Electric Energy Storage Systems for Transportation Electrification. His research interests include advanced power electronics, electric energy storage systems, and motor drives for transportation electrification.